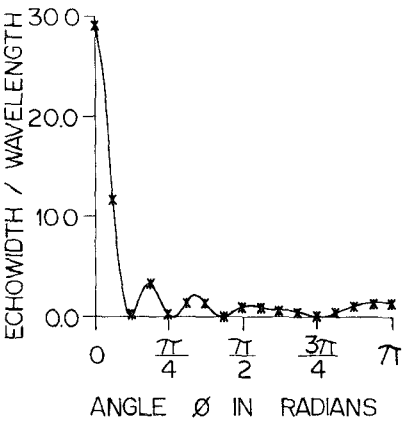

Fig. 2. Distant scattering pattern of a homogeneous cylindrical shell with an inhomogeneous patch — Method presented here * * * * Gaussian elimination method dielectric constant = $6.0 + j$ when $\phi = -\frac{7\pi}{128}$ to $\frac{7\pi}{128}$; = 3.0 elsewhere; mean radius = 1.0 λ, thickness = 0.05 λ number of cells = 128.

any case, when N is large and $L << N$, the overall computational effort is proportional to $N \log N$.

In comparison, the CGM-FFT method is $O(N^2 \log N)$, the Gaussian elimination method is $O(N^3)$. Thus, when N is large and $L << N$, the method presented here is significantly faster.

V. Numerical Results

The MM equations of the shell described in Fig. 2 were solved employing the Gaussian elimination method, the CGM-FFT method and the method presented here. The execution time for the three methods were 77550 msec, 9110 msec, and 561 msec, respectively. This includes the time for calculating the coefficients of the matrix. These results were obtained with Fortran 77 compiler on Toshiba T4400C notebook. Fig. 2 depicts the distant scattering pattern calculated from the solution of the MM equations. The exact agreement obtained verifies the correctness of the method proposed.

As a second example, a shell of mean radius 4.0λ and of the same thickness as the previous example was considered. The dielectric constant of the shell was taken to be 3.0 except in the region $-\frac{9\pi}{128} \leq \phi \leq \frac{9\pi}{128}$ where it was taken to be $6.0 + j$; the angle ϕ is as indicated in Fig. 1. The size of the MM matrix was 512 × 512; in the previous example it was 128 × 128. In view of the large size of the matrix, only the CGM-FFT method and the method presented here were implemented. The execution time for the two methods were 70 530 msec and 3350 msec, respectively. Thus, in both the cases, the method presented here was considerably faster.

VI. Conclusion

In this paper, we have presented a method for solving the MM equations of a circular, dielectric, cylindrical shell efficiently. Although we focused our attention on a homogeneous shell with a narrow inhomogeneous angular-region, the theory derived here does not assume that the perturbations should be contiguous; the method works even when there are more than one inhomogeneous patch. As the shell is a useful model for scatterers such as co-axial cables, volcanic pipes, blood vessels and arteries, efficient determination of the scattering pattern will be of use in applications such as crack detection.

References

[1] J. H. Richmond, "Scattering by a dielectric cylinder of arbitrary cross-section shape," *IEEE Trans. Antennas Propagat.*, vol. AP-13, pp. 334-341, May 1965.

[2] T K Sarkar, E. Arvas, and S M. Rao, "Application of FFT and the conjugate gradient method for the solution of electromagnetic radiation from electrically large and small conducting bodies," *IEEE Trans. Antennas Propagat.*, vol. AP-34, pp. 635-40, May 1986.

[3] M. F. Catedra, "Solution of some electromagnetic problems using the fast Fourier transform with conjugate gradient method," *Electronics Lett.*, vol. 22, pp. 1049-57, Sept. 25, 1986.

[4] J. D. Collins, J. L. Volakis, and J-M. Jin, "A combined finite element-boundary integral formulation for solution of 2-D scattering problems via CGFFT," *IEEE Trans. Antennas Propagat.*, vol. 38, pp. 1852-58, Nov. 1990.

[5] P. J. Davis, *Circulant Matrices*. New York Wiley, 1979.

[6] S. M. Kay, *Modern Spectral Estimation*. Englewood Cliffs, NJ: Prentice-Hall, 1988, ch. 1, pp. 3-25.

[7] J. G. Proakis, *Introduction to Digital Signal Processing*. New York: Macmillan, 1989.

Conductor-Loss Limited Stripline Resonator and Filters

Chen-Yu Chi and Gabriel M. Rebeiz

***Abstract*— We report on stripline resonators on thin dielectric membranes that show dispersion-free, conductor-loss limited performance at 13.5 GHz, 27.3 GHz, and 39.6 GHz. The unloaded-Q (Q_u) of the resonators increases as $\sqrt{f}$ with frequency and is measured to be 386 at 27 GHz. The measured results agree well with a new conformal mapping analysis. The stripline resonators are used in a micromachined state-of-the-art planar interdigitated bandpass filter at K-band frequencies. Excellent agreement has been achieved between the microwave model at 850 MHz and the 20 GHz filter. The micromachined filter exhibits a passband return loss better than −15 dB and a conductor-loss limited 1.7 dB port-to-port insertion loss (including input/output CPW line loss) at 20.3 GHz.**

I. Introduction

Silicon micromachined technology has been used recently to build low-loss lumped elements, K-band and W-band filters, resonators and couplers [1]–[3]. Micromachined components, suspended on thin dielectric membranes, do not suffer from dielectric and dispersion loss up to terahertz frequencies [4]. Also, with the advantage of the monolithic microwave/millimeter-wave integrated circuits (MMIC) fabrication process, batch fabricated micromachined components can have identical responses for use in large volume satellite receiver systems and future personal communication systems at microwave and millimeter-wave frequencies.

In this paper, we report on the performance of stripline and microstrip resonators on thin dielectric membranes at microwave and millimeter-wave frequencies. The stripline results are shown to be conductor-loss limited but the microstrip results show a small free-space radiation loss component at 13 GHz and this radiation loss

Manuscript received June 29, 1995; revised December 18, 1995. This work was supported by the National Science Foundation under the Presidential Young Investigator Award.

The authors are with the Electrical Engineering and Computer Science Department, University of Michigan, Ann Arbor, MI 48109-2122 USA

Publisher Item Identifier S 0018-9480(96)02339-3.

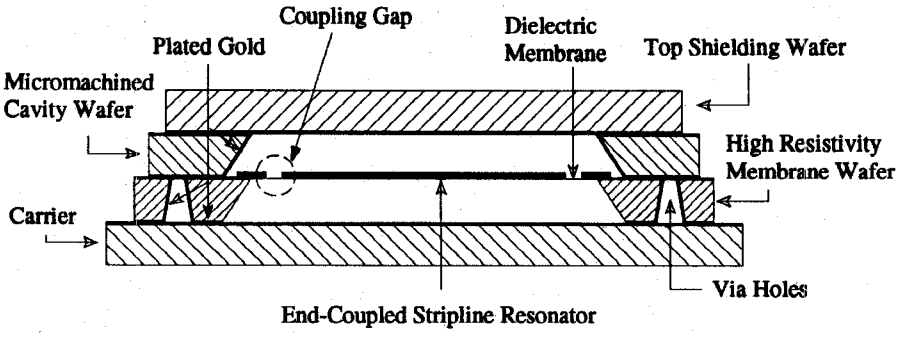

(a)

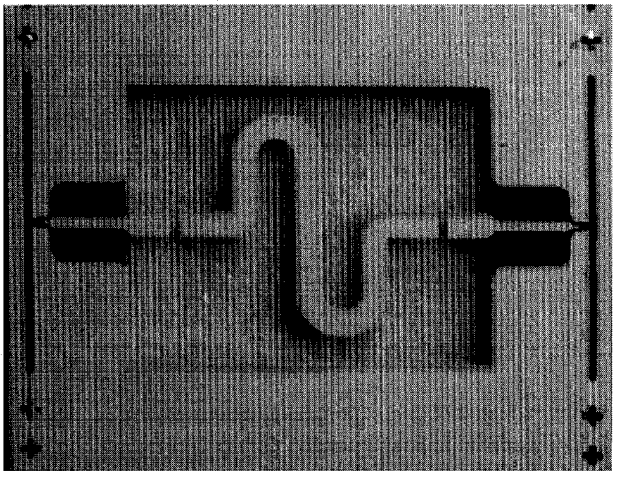

(b)

Fig. 1. (a) Cross-section view of the micromachined stripline resonator and (b) the fabricated resonator on a dielectric membrane.

becomes dominant at 40 GHz for the geometry considered herein. A 20 GHz interdigitated filter is then built using micromachined stripline technology. Excellent agreement is achieved between the microwave model at 850 MHz and the 20 GHz filter with a direct scaling and no resonator-length tuning due to the dispersion-free performance of micromachined striplines. The micromachined filter exhibits a return loss better than -15 dB within the passband and a conductor-loss limited 1.7 dB port-to-port insertion loss at 20.3 GHz.

II. Resonator Q-Measurements

The microstrip and stripline resonators are fabricated on a 350 μm-thick high-resistivity silicon wafer capped with a 1.4 μm dielectric membrane layer. A top shielding cavity is used in the case of the stripline resonators at a height of 350 μm above the resonator (Fig. 1). The top shielding cavity structure touches everywhere the membrane wafer except over the feeding grounded CPW-line (GCPW) where a channel is etched. The channel is 250 μm high, 1 mm wide, 1.5 mm long and provides RF microshielding of the feeding GCPW lines. Details of the fabrication process and the associated via-hole process around the dielectric membrane are presented in [1]. The microstrip and stripline resonator length is $\lambda_0/2$ at 13.5 GHz (1.1 cm) and is fabricated using standard lithography (Fig. 1). The resonator is 500 μm-wide and 3 μm-thick electroplated gold. The stripline resonator impedance is calculated to be 80.8 Ω and the microstrip resonator impedance is 104 Ω. The resonator is fed by 150 μm (and later by 220 μm) gaps in the feeding 50 Ω transmission line. The resonator Q-measurements with 150 μm and 220 μm feeding gaps gave very similar results.

Fig. 2 shows the measured S_{21} of the stripline and microstrip resonators with a feeding gap of 220 μm and 150 μm, respectively. The resonant frequencies for the stripline resonator are 13.555 GHz, 27.365 GHz, and 39.636 GHz [Fig. 2(a)], and are not exactly an integer multiple of each other because the gap-coupling capacitance changes with frequency [5]. Also, the peak S_{21} increases with frequency from -25.8 dB at 13.55 GHz to -10.4 dB at 39.36 GHz also due to the increase in the gap-coupling capacitance. The resonant frequencies for the microstrip resonator are 13.815 GHz, 27.163 GHz, and no resonant frequency is seen at 39 GHz due to radiation loss. Table I shows the measured loaded-Q (Q_L) and the extracted unloaded-Q (Q_u) using the following formulas [6]

$$Q_L = \frac{f_0}{(\Delta f)_{3dB}} \tag{1}$$

$$S_{21}(dB) = 10log_{10}\frac{Q_e^2}{Q_L^2} \tag{2}$$

and

$$\frac{1}{Q_L} = \frac{1}{Q_u} + \frac{1}{Q_e} \tag{3}$$

where Q_e is the external-Q of the resonator. It is defined as the Q of the resonator with its series resistance loss set to zero ($R_s = 0$) and the resistive loading of the resonator is due only to the loading effect.

As is evident in Table I, the stripline Q_u increases as $\sqrt{f}$ with frequency. This is an indication of conductor-loss limited performance and the absence of dielectric and radiation loss mechanisms. The attenuation (α_T) and the total series resistance (R_s) of the

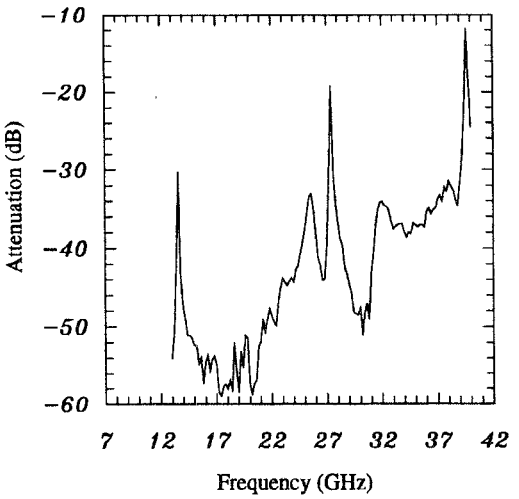

(a)

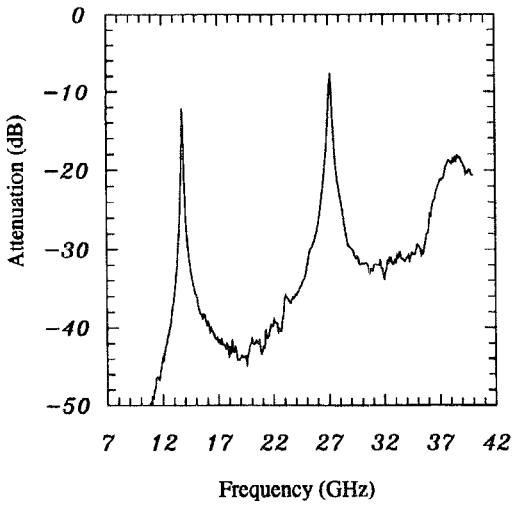

(b)

Fig. 2. Measured S_{21} of the micromachined resonator. (a) Stripline resonator. (b) Microstrip resonator.

TABLE I

	Stripline			Microstrip	
	f_{01}	f_{02}	f_{03}	f_{01}	f_{02}
	13.555	27.365	39.636	13.815	27.163
Q_L	258	331	304	155	110
Q_u	272	386	465	234	207
$Q_{u_f}/Q_{u_{f_{01}}}$	1	1.419	1.710	1	0.885
$\sqrt{f/f_{01}}$	1	1.421	1.710	1	1.402
Skin Depth (μm)	0.676	0.478	0.395	0.676	0.478
$\alpha_T(NP/cm)$	0.0052	0.0074	0.0089	0.0062	0.0137
$R_s(\Omega/cm)$	0.841	1.196	1.439	1.286	2.858
$R_s(\Omega/cm)$ *Linecalc*	0.634	0.949	1.166	-	-
$R_s(\Omega/cm)$ *IE3D*	0.861	1.272	1.565	-	-
$R_s(\Omega/cm)$ *Conformal Mapping*	0.762	1.153	1.410	-	-

micromachined stripline is calculated from the extracted unloaded-Q assuming conductor-loss limited performance and using

$$\alpha_T = \frac{\pi}{Q_u \lambda} = \frac{R_s}{2Z_0} \tag{4}$$

where Z_0 is the characteristic impedance of the resonator. The same stripline geometries are analyzed by using three different techniques: quasi-static analysis, method-of-moment (MoM), and a new conformal mapping technique developed by E. Tuncer *et al.* [7]. The quasi-static analysis here is performed by the EESof Linecalc^{TM} caculation and the method-of-moment analysis is performed by the IE3D^{TM} program [8]. The conformal mapping technique uses an isolated-conductor surface impedance in conjunction with a conformal map for the entire transmission line cross section to account for both skin-depth and current crowding effect [7]. Therefore, the conformal mapping model can more accurately predict the series impedance of a transmission line for a conductor with finite conductivity. The MoM method can also predict the series resistance from the finite conductivity of the metal used. However, due to the current crowding effect at the edge of the stripline, the MoM results are strongly depend on the grid size which is used to partition the cross section of the stripline. The quasi-static analysis cannot take the current crowding effect into account, therefore, a smaller series resistance can be expected from this analysis. The predicted series resistances from these three techniques are also listed in Table I. As can be seen, excellent agreements are achieved between the measured results and the conformal mapping technique. The stripline resonators are ideal for millimeter-wave applications (30-300 GHz) since their unloaded-Q increases with frequency. In this case, care should be taken on not to induce higher-order modes in the stripline cavity.

On the other hand, the microstrip line resonator suffers from radiation loss and its unloaded-Q decreases with frequency. The 13 GHz Q_u is 235 and is about 15% less than the stripline resonator due to a small component of radiation loss. At 27 GHz, the radiation loss component is comparable to the conductor-loss component resulting in $Q_u = 205$ which is around half the value of the stripline resonator at this frequency. At 39 GHz, the radiation loss is very high and no Q-measurements could be done. It is possible to reduce the radiation loss by decreasing the height of the substrate or by increasing the width of the microstrip line.

III. 20 GHz Stripline Bandpass Filter

The design procedure of an interdigitated stripline filter has been developed by Matthaei [6] and [9]. In this work, only the coupling between adjacent resonators has been considered in the admittance/impedance matrices, and a bandwidth correction factor is needed to compensate for neglecting the mutual coupling between the nonadjacent resonators. The stripline interdigitated filter is built on a very thin dielectric membrane (1.5 μm thick) and results in a pure TEM propagation mode with no dispersion effects. Because of the pure TEM mode, a microwave model can yield accurate simulation of the performance of the 20 GHz filter. Based on this concept, an 850 MHz microwave model is built with a scaling factor of 23.7. The resonators and ground plane in the microwave model are made of copper tape. Matthaei's equations [6], [9] were first used as a starting point and then the lengths, widths, and gaps of the eight finger-resonators were adjusted experimentally. The microwave model show a center frequency of 856 MHz and a 3-dB bandwidth of 140 MHz and a port-to-port insertion loss of 0.7 dB (including 0.3 dB from the input/output coaxial cables). This translates into a center frequency of 20.28 GHz with a 3-dB bandwidth of 3.3 GHz for the micromachined filter.

A 20 GHz is then fabricated using the same technology described in [1] and is shown in Fig. 3 with its associated dimensions. The membrane cavity is surrounded by a row of via-holes to ensure proper grounding. The input line is a grounded-CPW line and is 2.6 mm long. A micromachined cavity wafer with a mouse-hole channel is stacked on top of the membrane wafer using silver epoxy and this

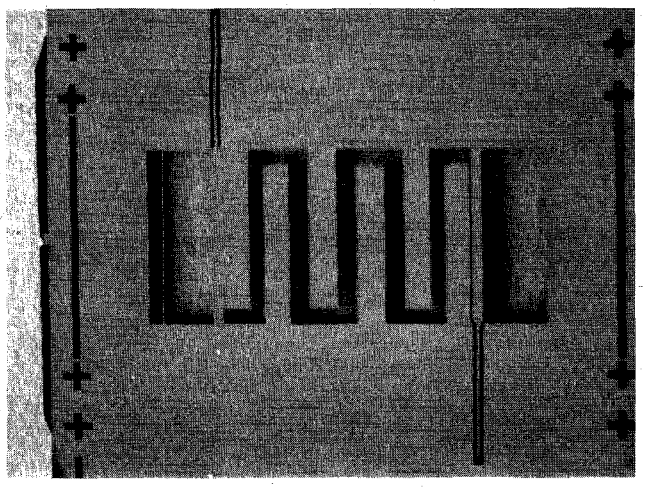

(a)

K	$s_{k,k+1}(\mu m)$	K	$w_k(\mu m)$	$l_k(\mu m)$
0, 6	23	0, 7	229	3373
1, 5	285	1, 6	503	3112
2, 4	371	2, 5	528	3101
3	376	3, 4	577	3086
K: finger number			w_k: finger width	
$s_{k,k+1}$: gap between fingers			L_k: finger length	

(b)

Fig. 3. The 20 GHz interdigitated membrane filter (a) Its physical dimensions [1]. (b) The clear area on this picture is the dielectric membrane.

creates the top cavity for the filter. Another carrier wafer is stacked at bottom of the membrane wafer to form the bottom cavity. Both the top cavity and bottom carrier wafer are electroplated with gold to obtain a good RF ground plane.

A 20 μm diameter gold wire is bonded across the first finger at the membrane-GCPW transition to equalize the two ground planes of the GCPW line. The bonding wire is important because it forces a symmetrical field distribution at the transition and provides a 50 Ω feeding impedance at the GCPW line. This filter is measured from 2 to 40 GHz and no tuning is attempted during the measurements. The results show a 1.7 dB port-to-port insertion loss at 20.3 GHz (including a 0.3 dB loss from each of the GCPW line) with a 3-dB bandwidth of 3.1 GHz (Fig. 4). The return loss is better than -15 dB in the passband. As can be seen, excellent agreement is achieved between the 850 MHz design and the 20.3 GHz results due to the TEM nature of the micromachined filter (no dispersion effects).

The measured resonator has a Q_u of 272 at 13.5 GHz and this translates to a Q_u of 331 at 20 GHz. The 3-dB bandwidth of this filter is about 15%. Using these parameters, the insertion loss of the 20 GHz filter can be calculated using the following equation [6]

$$\Delta L_A(dB) \simeq 8.686 C_n \frac{1}{\omega Q_u} \tag{5}$$

where ω is the fractional bandwidth of the bandpass filter and C_n is a tabular constant given in [6] and is equal to 4.5.

The insertion loss of the 20 GHz filter from the resonators along is calculated to be 0.79 dB. The input mismatch $S_{11} = -15$ dB contributes 0.14 dB loss to the total insertion loss. Also, the GCPW feeding structures add another 0.6 dB (0.3 dB from each side of the feeding structure) into the total insertion loss of the filter. The calculated port-to-port insertion loss is therefore 1.53 dB which is very closed to the measured value of 1.7 dB.

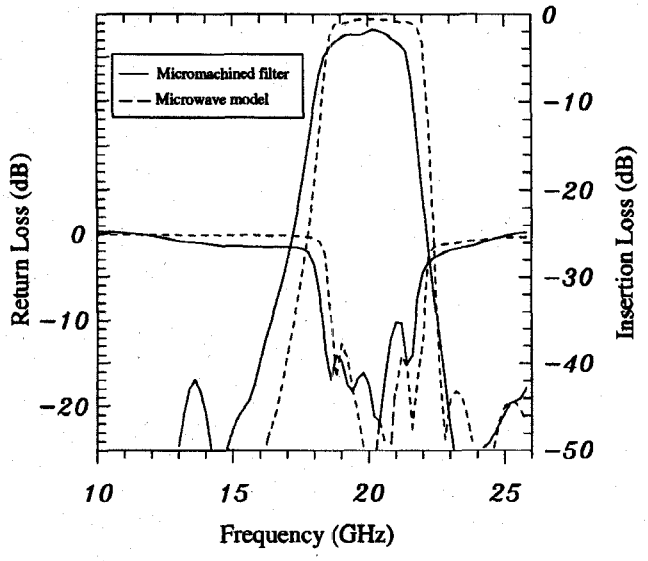

Fig. 4. Measured response for the 20 GHz micromachined interdigitated filter.

Fig. 4 shows a small discrepancy between the 850 MHz model and the 20 GHz filter. The mechanism which accounts for this is due to the quality factor Q of each resonator. In the 850 MHz model, the resonators are 23.7 (scaling factor) times wider than the resonators used in the 20 GHz filter. Therefore, the resonator-Q in the 850 MHz model is 4.87 ($\sqrt{23.7}$) times larger than the resonator-Q in the 20 GHz filter. The higher Q in the microwave model results in a passband loss of 0.16 dB and provides a sharper out-of-band rejection. The measured total insertion loss in the microwave model (0.7 dB) agrees well with the expected value of 0.6 dB (0.16 dB; resonator loss, 0.14 dB; S_{11} loss, and 0.3 dB; coaxial cable loss).

IV. Conclusion

We report on the measured quality factor Q of membrane suspended stripline resonators. The quality factor (Q_u) in this structure shows a conductor-loss limited performance and increases as $\sqrt{f}$ with frequency. The measured results agree very well with a loss analysis from the conformal mapping technique. Based on the Q-measurements, a 20 GHz stripline interdigitated filter was built. The RF characteristic of the 20 GHz filter were well predicted from the Q-measurements and a microwave model due to the dispersion-free performance. The stripline resonators are ideal for use in planar high quality microwave and millimeter-wave filters and components.

Acknowledgment

The authors would like to thank D. P. Neikirk and B.-T. Lee at the University of Texas, Austin, for performing the conformal mapping caculation.

References

[1] C. Y. Chi and G. M. Rebeiz, "Planar microwave and millimeter-wave lumped elements and coupled-line filters using micro-machining techniques," *IEEE Trans. Microwave Theory Tech.*, vol. 43, no. 4, pp. 730–738, Apr. 1995.

[2] S. V. Robertson, L. P. B. Katehi and G. M. Rebeiz, "Micromachined self-packaged W-band bandpass filters,"*1995 IEEE MTT-S Int. Microwave Symp.*, vol. 3, May 1995, pp. 1543–1546.

[3] T. M. Weller, L. P. B. Katehi, and G. M. Rebeiz, "High performance microshield line components," *IEEE Trans. Microwave Theory Tech.*, vol. 43, no. 3, pp. 534–543, Mar. 1995.

[4] H. Cheng, J. F. Whitaker, T. M. Weller, and L. P. B. Katehi, "Terahertz-bandwidth characterization of coplanar waveguide via time-domain electro-optic sampling," in *1994 IEEE MTT-S Int. Microwave Symp.*, vol. 1, May 1994, pp. 477-480.
[5] H. M. Altschuler and A. A. Oliner, "Discontinuities in the center conductor of symmetric strip transmission line," *IRE Trans. Microwave Theory Tech*, vol. MTT-8, pp. 328–339, May 1960.
[6] G. L. Matthaei, L. Young, and E. M. T. Jones, *Microwave Filters, Impedance-Matching Networks, and Coupling Structures.* Norwood, MA: Artech House, 1980, ch. 11, pp. 651–723.
[7] E. Tuncer, B. T. Lee, M. S. Islam, and D. P. Neikirk, "Quasi-static conductor loss calculations in transmission lines using a new conformal mapping technique," *IEEE Trans. Microwave Theory Tech.*, vol. 42, pp. 1807–1815, Sept. 1994.
[8] IE3D Version 2.1, Zeland Software, Inc., Fermont, CA 94538.
[9] G. L. Matthaei, "Interdigital band-pass filters," *IRE Trans. Microwave Theory Tech.*, vol. MTT-10, pp. 479–491, Nov. 1962.

Color Group Approach to Symmetrical Ferrite Devices with Polarization Effects

Victor A. Dmitriyev

***Abstract*— Applicability of the color group approach to symmetrical ferrite devices with polarization effects is demonstrated. By using the theory of symmetry, the scattering matrices of square and circular waveguides with quadrupole dc magnetic field are derived.**

The color (magnetic) group approach proposed in [1] is also applicable to symmetrical ferrite devices with polarization effects. To demonstrate this possibility, let us consider a square quadrupole gyromagnetic waveguide depicted in Fig. 1.

We shall use here a description of the waveguide in terms of a pair of orthogonal coupled modes [2] with the port nomenclature, illustrated in Fig. 1(b).

The square waveguide is described by the group of symmetry D_{4h} in Schoenflies notation [3]. The quadrupole dc magnetic field has the symmetry $D_{4h}(D_{2d})$. Hence, the magnetic group of symmetry of the system "waveguide + dc magnetic field" is $D_{4h}(D_{2d})$, and the group consists of 16 elements:

E	Identity operation.
S_{4z}, S_{4z}^{-1}	Improper rotation about z-axis by $\pi/2$ and $-\pi/2$, respectively.
C_{2z}	Rotation about z-axis by π.
$\sigma(a\text{-}a), \sigma(b\text{-}b)$	Reflection in the planes passing through the waveguide axis and the axes $(a\text{-}a)$ and $(b\text{-}b)$, respectively.
C_{2x}, C_{2y}	Rotation by π about x- and y-axis, respectively.
TC_{4z}, TC_{4z}^{-1}	Antirotation about z-axis by $\pi/2$ and $-\pi/2$, respectively.
$TC_{2(a-a)}, TC_{2(b-b)}$	Antirotation by π about a-a and b-b axes, respectively.
$T\sigma_x, T\sigma_y$	Antireflection in the planes $x = 0$ and $y = 0$, respectively.
$T\sigma_z$	Antireflection in the plane $z = 0$.
T_I	Anti-inversion.

Manuscript received July 26, 1995; revised December 18, 1995.
The author is with the Army Politechnical School, Quito, Equador.
Publisher Item Identifier S 0018-9480(96)02337-X.

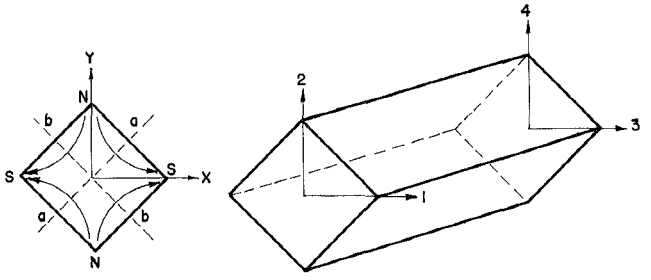

Fig. 1. Schematic diagram of square waveguide with a quadrupole dc magnetic field.

Here T denotes the operation of time reversal.

Generators of the group may be, for example, $C_{2x}, \sigma_{(a-a)}$ and $T\sigma_z$. The corresponding symmetry operators of the quadrupole gyromagnetic waveguide are

$$[R]_{C_{2z}} = \begin{vmatrix} 0 & 0 & 1 & 0 \\ 0 & 0 & 0 & -1 \\ 1 & 0 & 0 & 0 \\ 0 & -1 & 0 & 0 \end{vmatrix}; \quad [R]_{\sigma_{(a-a)}} = \begin{vmatrix} 0 & 1 & 0 & 0 \\ 1 & 0 & 0 & 0 \\ 0 & 0 & 0 & 1 \\ 0 & 0 & 1 & 0 \end{vmatrix};$$

$$[R]_{T\sigma_z} = \begin{vmatrix} 0 & 0 & 1 & 0 \\ 0 & 0 & 0 & 1 \\ 1 & 0 & 0 & 0 \\ 0 & 1 & 0 & 0 \end{vmatrix}.$$

Using the following commutation relations

$$[R]_{C_{2x}}[S] = [S][R]_{C_{2x}},$$
$$[R]_{\sigma_{(a-a)}}[S] = [S][R]_{\sigma_{(a-a)}},$$
$$[R]_{T\sigma_Z}[S] = [S]^t[R]_{T\sigma_z},$$

where t denotes transposition, we get the matrix $[S]$

$$[S] = \begin{vmatrix} S_{11} & 0 & S_{13} & S_{14} \\ 0 & S_{11} & S_{14} & S_{13} \\ S_{13} & -S_{14} & S_{11} & 0 \\ -S_{14} & S_{13} & 0 & S_{11} \end{vmatrix}. \tag{1}$$

The matrix $[S]$ has three independent complex parameters. The quantities S_{ij} depend on the parameters of the waveguide and its length. Notice that in the matrix (1) $S_{13} = S_{31}, S_{24} = S_{42}$, because the pairs of the ports 1, 3 and 2, 4 lie in the antiplanes of symmetry $y = 0$ and $x = 0$, respectively. It is in accordance with the theory suggested in [1]. The ports 1 and 2, and also 3 and 4 are completely decoupled from each other.

If $S_{11} = 0$, we get the scattering matrix for the ideally matched waveguide. Then, using the unitary conditions

$$[S][S^*]^t = [E] = [S^*]^t[S]$$

we get the matrix $[S]$ for the waveguide without losses

$$[S] = \begin{vmatrix} 0 & 0 & k & \pm j\sqrt{1-k^2} \\ 0 & 0 & \pm j\sqrt{1-k^2} & k \\ k & \mp j\sqrt{1-k^2} & 0 & 0 \\ \mp j\sqrt{1-k^2} & k & 0 & 0 \end{vmatrix}. \tag{2}$$

This matrix describes a nonreciprocal directional coupler. Here, with properly chosen terminal surfaces, $k = S_{13}$ is real. The upper